Geophysical Research Letters

RESEARCH LETTER
10.1029/2020GL091674

Early Warning of the Pacific Decadal Oscillation Phase Transition Using Complex Network Analysis

Zhenghui Lu[1], Naiming Yuan[2,3,4], Qing Yang[1], Zhuguo Ma[1,5], and Jürgen Kurths[6,7,8]

[1]CAS Key Laboratory of Regional Climate Environment for Temperate East Asia, Institute of Atmospheric Physics, Chinese Academy of Sciences, Beijing, China, [2]School of Atmospheric Sciences, Sun Yat-Sen University, Zhuhai, China, [3]Key Laboratory of Tropical Atmosphere-Ocean System, Ministry of Education, Zhuhai, China, [4]Southern Marine Science and Engineering Guangdong Laboratory, Zhuhai, China, [5]University of Chinese Academy of Sciences, Beijing, China, [6]Department of Physics, Humboldt University, Berlin, Germany, [7]Potsdam Institute for Climate Impact Research, Potsdam, Germany, [8]Lobachevsky University of Nizhny Novgorod, Nizhny Novgorod, Russia

Abstract Obtaining an efficient prediction of the Pacific Decadal Oscillation (PDO) phase transition is a worldwide challenge. Here, we employed the climate network analysis to uncover early warning signals prior to a PDO phase transition. This way an examination of cooperative behavior in the PDO region revealed an enhanced signal that propagated from the western Pacific to the northwest coast of North America. The detection of this signal corresponds very well to the time when the upper ocean heat content in the off-equatorial northwestern tropical Pacific reaches a threshold, in which case a PDO phase transition may be expected with the arising of the next El Ni $\tilde{n}$o/La Ni$\tilde{n}$ a event. The objectively detected early warning signal successfully forewarned all the six PDO phase transitions from the 1890–2000, and also underpinned the possible PDO phase transition around 2015, which may be triggered by the strong El Ni$\tilde{n}$o event in 2015–2016.

Plain Language Summary The Pacific Decadal Oscillation (PDO), as one of the main internal decadal climate variabilities, has been shown to have substantial impacts on both the climate system and other parts of Earth system. Due to its complexity, however, it is still challenging to predict its phase changes. Here, a new technique from climate network analysis was employed to capture the potential precursors of the phase transition. By calculating the linkages between the warm and cold regions of the PDO spatial pattern, a sudden strengthening of negative connections between the two regions was detected a few years before the phase transition. This early warning signal arises from the cooperative behavior of the considered regions, that is, many more grid points from the two regions are becoming negatively linked at the time of alarming. This time corresponds well to the moment when the upper ocean heat content in the off-equatorial northwestern tropical Pacific reaches a threshold, in which case a PDO phase transition may be expected with the arising of the next El Ni$\tilde{n}$o/La Ni$\tilde{n}$a event. Since the early warning signal is objectively detected from the climate network analysis, it may be used in operations for improved predictions of the PDO.

Key Points:

- An early warning signal for the Pacific Decadal Oscillation (PDO) phase transition is detected
- The signal arises mainly from the cooperative behaviors of the grid points in the PDO region
- A new strategy for the prediction of the PDO phase transition is proposed

Supporting Information:

Supporting Information may be found in the online version of this article.

Correspondence to:

N. Yuan,
naimingyuan@hotmail.com

Citation:

Lu, Z., Yuan, N., Yang, Q., Ma, Z., & Kurths, J. (2021). Early warning of the Pacific Decadal Oscillation phase transition using complex network analysis. *Geophysical Research Letters*, *48*, e2020GL091674. https://doi.org/10.1029/2020GL091674

Received 12 NOV 2020
Accepted 31 JAN 2021

1. Introduction

The Pacific Decadal Oscillation (PDO), defined as the leading sea surface temperature (SST) pattern in the North Pacific poleward of 20°N, has been recognized as one of the main patterns that represents the internal decadal climate variability (DCV, Mantua et al., 1997). It has been shown to have substantial impacts not only on the climate system (Cai & van Rensch, 2012; Newman et al., 2016; Qian & Zhou, 2013; Yang et al., 2017), but also on other areas of the Earth system, including agriculture, natural resources, and ecosystems (Boulton & Lenton, 2015). In particular, the modulation effects of the PDO on long-term warming trends due to increasing anthropogenic greenhouse gases (GHGs, Dai et al., 2015; Medhaug et al., 2017) make the understanding and predicting the PDO a challenging task that has got strong attention.

As a phenomenon with time scales of 15–25 years and 50–70 years, the PDO is found not to be a single physical mode, but a combination of multiple processes of different origins (Newman et al., 2016). Most discussed drivers include: (a) stochastic forcings generated by both local atmospheric noise, and remote forcings due to tropical variabilities (e.g., ENSO events, Newman et al., 2003; Pierce, 2001; Schneider &

Cornuelle, 2005); (b) tropical-subtropical interactions via atmospheric and oceanic responses (Alexander et al., 2002; Deser et al., 2004; Liu & Alexander, 2007); and (c) ocean dynamics, such as oceanic reemergence (Alexander et al., 1999; Schneider & Cornuelle, 2005) and ocean gyre dynamics (Newman et al., 2016). However, how these processes are integrated and their roles in driving the PDO is still unclear due to the lack of long-term reliable observations and the complexity of the system. As a result, it is challenging to model and predict the PDO, especially the PDO phase transition (Cassou et al., 2018). In current coupled models, the spatial characteristics of the PDO may be roughly captured (Henley et al., 2017; Sheffield et al., 2013), but its temporal variations are poorly reflected and there remain large intermodel uncertainties (Newman et al., 2016). After proper initialization, the simulations may be improved for a few initial years (Meehl et al., 2014; Mochizuki et al., 2010), but compared to other regions, the simulation in the northern Pacific is found to have the lowest skill in initialized near-term climate predictions (Doblas-Reyes et al., 2013). A successful prediction of the PDO phase transition relies on simulations of the relevant processes, which so far are still difficult (Farneti, 2017). In addition, efforts have also been made to predict the regime duration based on the persistence of different processes (Mantua & Hare, 2002; Newman et al., 2016). However, the corresponding prediction errors increase rapidly, and the predictive skill disappears when a PDO phase transition occurs (Mantua & Hare, 2002; Mochizuki et al., 2010). There are also other approaches utilizing statistical analyses (Chylek et al., 2014; Henley, 2017; Landscheidt, 2001), which are verified by a few successful phase transition predictions, but lack a physical basis and the instability is questionable.

A primary reason for this current dilemma in PDO prediction is that the PDO is not a single physical mode. The interactions of multiple processes of different origins and the subsequent nonlinear effects dramatically increase the complexity and randomness of the system. For instance, a PDO phase transition may be largely randomly forced due to variations in coupled relevant processes (Newman et al., 2016), and the potential precursors may be too weak to be traced. Therefore, besides the continuous efforts for the development of coupled models, novel approaches based on advanced mathematical/physical concepts also deserve attention. In recent years, complex network analysis (Boers et al., 2019; Radebach et al., 2013; Tsonis et al., 2006), has been shown to have a strong potential to detect precursors of major climatic events. In climate, it is also called climate network analysis. This new approach takes the grid points in climate system as nodes, and the interactions between each pair of the nodes as links. In the analysis, since the complex system as a whole with all of the interior grid points is properly considered, a weak negligible signal may stand out if a large number of grid points behave similarly (cooperative behavior). The climate network analysis has been successfully applied in: (1) warning of the emergence of El Niño events even one year in advance (Ludescher et al., 2013; Meng et al., 2020); (2) forecasting changes in the Atlantic Meridional Overturning Circulation (AMOC, Feng et al., 2014; van der Mheen et al., 2013); and (3) predicting the paths of extreme precipitation (Boers et al., 2014). In this study, we will employ it to investigate whether the phase transition of the PDO can be forewarned from this new perspective.

The rest of the paper is organized as follows. In Section 2, we will briefly introduce the data and the methods (including how to construct a climate network and the metrics of interest) used in this paper. In Section 3, an early warning signal will be described, and the associated cooperative effects will be shown. After a further investigation of the underlying physical meanings of the early warning signal, we propose a new strategy for the prediction of the PDO phase transition, and conclude this paper in Section 4.

2. Data and Methods

2.1. Data

In this study, monthly sea surface temperature anomalies (SSTA) from 1854 to 2018 over the North Pacific between 120°E and 120°W, 20°N and 60°N were analyzed. The data were obtained from the Extended Reconstructed Sea Surface Temperature (ERSST) data set (Version 3b, Smith et al., 2008), and the horizontal resolution selected for analysis is 4°×°4 (277 grid points in total). According to the definition of the PDO, the empirical orthogonal function (EOF) analysis is first applied to these monthly SSTA data. The first EOF spatial distribution pattern and its corresponding time series (Figure S1) are identified as the spatial pattern of the PDO and the PDO index, respectively. Next, the border that divides the north Pacific into warm/cold regions is determined based on its spatial pattern. As shown in Figure 1a, the area along the west coast of the Americas is marked as region "*B*" (110 grid points), and the residual central north Pacific is marked as region

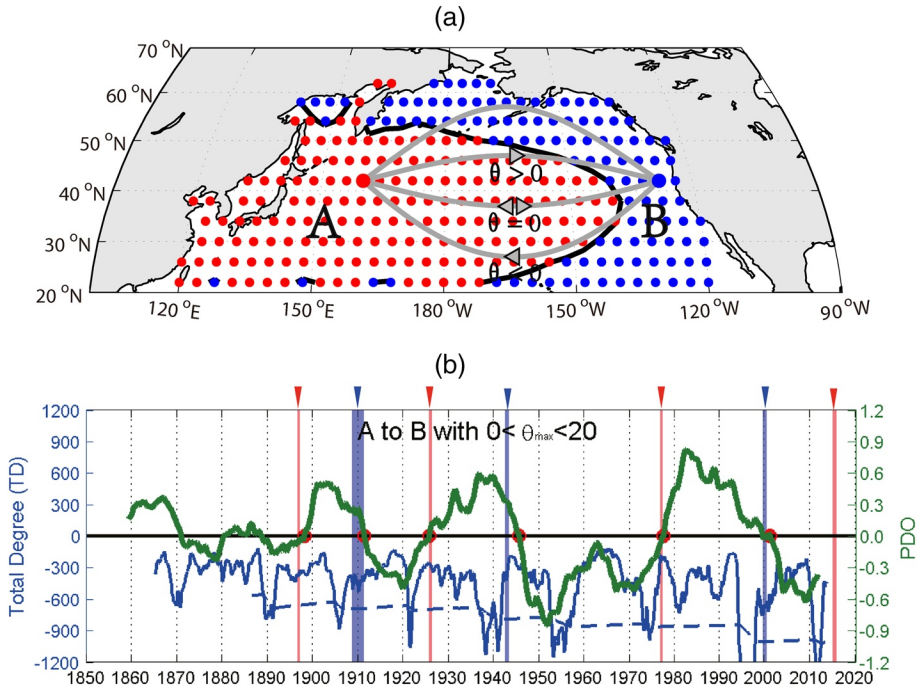

Figure 1. (a) The constructed climate network in the north Pacific. The regions "*A*" and "*B*" were determined according to the definition of the PDO. The gray lines show the potential links between nodes in "*A*" and nodes in "*B*". For $\theta > 0$, the link points from "*A*" to "*B*". For $\theta < 0$, the link points from "*B*" to "*A*". If $\theta = 0$, the sea surface temperature anomalies in both nodes vary simultaneously. (b) Relations between the 11-years running mean PDO index (green) and the total degrees (negative links) pointed from "*A*" to "*B*", $TD_{A\to B}$ (blue). The dashed line represents the threshold that determines whether the $TD_{A\to B}$ decrease is significant. The red/blue vertical bars as well as the triangular symbols on the top of the subfigure mark the El Niño/La Niña events that may trigger the PDO phase transition, following the theory proposed by (Meehl et al., 2016; Meehl & Hu, 2006). PDO, Pacific decadal oscillation.

"*A*" (167 grid points). Considering the large interdecadal oscillations in the PDO index, an 11-years running mean was calculated to extract the decadal variability of the PDO. In addition to the SST data, the monthly sea subsurface temperature data obtained from Institute of Atmospheric Physics (IAP) were also used in this work. The data features global coverage of oceans at 1°×°1 horizontal resolution on 41 vertical levels (1–2000 m) with the temporal length from 1940 to 2018 (Cheng et al., 2017). Here we only analyzed the data after 1965 due to its big uncertainty before 1960 caused bydifferent temperature measurements (Ishii & Kimoto, 2009).

2.2. Methods

2.2.1. Climate Network

In the region of interest (Figure 1a), each grid point is regarded as a node and the corresponding network is constructed by determining the links among the nodes. In this study, we employed the Pearson correlation analysis to calculate the links (Tsonis et al., 2006). For each node k, we first extracted the SSTA by subtracting long-term mean annual cycle for every 30 years before a considered time point t, and removed the global average to obtain its temperature anomaly $T_k(t)$. For each pair of nodes between region "*A*" and "*B*", we computed for each month t, the cross-correlations with time lags of $-80 < \theta < 80$ months, as shown below,

$$C^t_{i,j}(0) = \begin{cases} \dfrac{\langle T_i(t-\theta)T_j(t)\rangle - \langle T_i(t-\theta)\rangle\langle T_j(t)\rangle}{\sqrt{\left\langle \left(T_i(t-\theta) - \langle T_i(t-\theta)\rangle\right)^2\right\rangle \left\langle \left(T_j(t) - \langle T_j(t)\rangle\right)^2\right\rangle}}, \theta > 0, A \to B \\ \dfrac{\langle T_i(t)T_j(t+\theta)\rangle - \langle T_i(t)\rangle\langle T_j(t+\theta)\rangle}{\sqrt{\left\langle \left(T_i(t) - \langle T_i(t)\rangle\right)^2\right\rangle \left\langle \left(T_j(t+\theta) - \langle T_j(t+\theta)\rangle\right)^2\right\rangle}}, \theta < 0, B \to A \end{cases}, \quad (1)$$

where i represents a node in "A" and j stands for a node in "B". Since we used an 11-years (132 months) running mean index to show the decadal variability of the PDO, to ensure that the calculated links and the PDO index share the same time interval, we chose 66 months (5.5 years) after the considered time point t as a window to calculate the correlations. The brackets in Equation 1 denote an average over this window. By moving the window, time-varying correlations can be obtained. For each time point t, the link strength $C^t_{i,j}\left(\theta_{\max}\right)$ is defined as the maximum absolute cross-correlation among the 161 coefficients ($-80 < \theta < 80$ months), and the θ_{max} determines the link direction. If $\theta_{max} = 0$, node i from "A" and node j from "B" are simultaneous. If $\theta_{max} > 0$, then the link points from i to j, and vice versa (Figure 1a). In this way, a directed climate network that describes how the two regions "A" and "B" are connected, is constructed.

2.2.2. Metrics of Interest

Based on the constructed climate network, a series of metrics of interest can be calculated in a window-wise analysis (i.e., getting the time-varying metrics). First, for a given node i in "A", by summing all the links connected with the nodes in "B", the so-called node degree (Tsonis et al., 2006) is determined as,

$$K_i\left(t\right) = \sum_{j\in B} C^t_{i,j}\left(\theta_{\max}\right) \tag{2}$$

This equation also applies for the calculation of node degrees in "B". Furthermore, the total degree (Radebach et al., 2013) between the two regions is defined as,

$$TD\left(t\right) = \sum_{i\in A,\, j\in B} C^t_{i,j}\left(\theta_{\max}\right) \tag{3}$$

which measures how the two regions are linked with each other. If the link directions are considered, by summing the links with $\theta_{max} > 0$, the total degrees from "A" to "B" (i.e., $TD_{A\to B}$) can be calculated. While by summing the links with $\theta_{max} < 0$, the total degrees from "B" to "A" (i.e., $TD_{B\to A}$) can be obtained. It is worth noting that, the links can be either positive or negative, depending on the signs of the maximum cross-correlations. In this study, the negative links were mainly considered and the degrees from "A" to "B" were calculated by summing the links with $0 < \theta_{max} < 20$ months (Figure S2). The results based on positive links were shown in the supporting information.

In addition to the degrees, the number of links that connects "A" and "B" is also a metric of interest. For a given node i in "A", the number of links at time point "t" can be easily calculated as

$$N_i\left(t\right) = \sum_{j\in B} n^t_{i,j} \tag{4}$$

where $n^t_{i,j}$ denotes whether the node i in "A" is linked with the node j in "B". If there is a link, $n^t_{i,j} = 1$, otherwise it equals zero. By setting different conditions for $n^t_{i,j}$, one can count different types of links. For instance, if only links with $\theta_{max} > 0$ are considered, then $N_i(t)$ gives the number of out-going links from i in "A" to region "B". Similarly, one could also count the number of in-coming links ($\theta_{max} < 0$), negative links $\left(C^t_{i,j}\left(\theta_{\max}\right) < 0\right)$, positive links $\left(C^t_{i,j}\left(\theta_{\max}\right) > 0\right)$, etc. It is worth nothing that in climate network theories, $N_i(t)$ is also considered as a kind of "node degree", but unlike $K_i(t)$, it is unweighted. To avoid confusing $N_i(t)$ with $K_i(t)$, we name $N_i(t)$ here as the number of links. By further calculating the ratio of $K_i(t)$ to $N_i(t)$, as shown in Equation 5,

$$S_i\left(t\right) = \frac{K_i\left(t\right)}{N_i\left(t\right)} \tag{5}$$

one could also measure the average strength of links. These calculations also applies for the nodes in region "B". In this work, we will use these metrics to detect the cooperative behaviors among the nodes in the climate network.

3. Results

3.1. Detecting an Early Warning Signal

Since the PDO phase transition is a seesaw-like change of SSTA in regions "A" and "B", it is essential to investigate, from the climate network perspective, how these two regions are linked and whether these linkages change prior to a phase transition. Using Equations 1 and 2, we mainly focused on the negative links (identified from anticorrelations) between nodes in "A" and nodes in "B". By counting all the negative links (Figure S2), we find that, although for most cases the strongest correlations occurred at $\theta_{max} = 0$ (simultaneous), there were quite a few cases with the strongest correlations at a delay of $0 < \theta_{max} < 20$ months ("A" points to "B") and $-20 < \theta_{max} < 0$ months ("B" points to "A"), indicating potential teleconnections between "A" and "B" (see Figure S3). By combining all the negative links with $0 < \theta_{max} < 20$ months, the total degree ($TD_{A\to B}$) is defined as the sum of the link strengths (Equation 3). This way, we find a very good connection between variations in the $TD_{A\to B}$ and the PDO phase transition. When there was a PDO phase transition, a sharp decrease in the $TD_{A\to B}$ always appeared a few years in advance (Figure 1b). This finding is further confirmed by the node degree evolutions during a PDO cycle (see Figures S4 and S5), suggesting a sudden strengthening of the anticorrelation between region "A" and region "B" and "A" led "B" by 0 ~20 months. In view of the poor data quality in the 1800, only the six clear PDO phase transitions after 1890 are included (the red points in Figure 1b), and significant $TD_{A\to B}$ decreases are found for all of the six cases (the threshold $TD_H(t)$, shown as the dashed blue line in Figure 1b is defined as the lower bound of the two times standard deviations of $TD_{A\to B}$, that is calculated using $TD_{A\to B}$ from the beginning time to the current time t). If the significant decrease of $TD_{A\to B}$ is regarded as an early warning signal for a PDO phase transition, taking the first time point when $TD_{A\to B}$ exceeds TD_H as the warning point, seven alarms sounded from 1890 to 2000, and six of them correctly warned of a PDO phase transition with an average of 6.5 ± 2.3 years in advance. This is in line with the estimated upper limit of the PDO predictability time, which is around 7–9 years (Li et al., 2020; Newman et al., 2016). There is only one false alarm sounded in the middle of the 1950. However, it should be noted that the PDO index in the following years climbed upward gradually until the beginning of 1960, which had almost formed a phase transition. The index TD for the negative links with $-20 < \theta_{max} < 0$ months ("B" points to "A") were also analyzed, but no clear connections between the $TD_{B\to A}$ and the PDO phase transition were revealed (see Figure S6). In addition, the results based on positive links can be found in the supporting information (Figures S7 and S8).

3.2. Understanding the Early Warning Signal

To check whether the $TD_{A\to B}$ can be used as a meaningful early warning signal, here we conducted a composite analysis. First the time points are classified into two groups: an "Anomaly" group and a "Normal" group. In the "Anomaly" group, all of the time points with a $TD_{A\to B}$ lower than the threshold (Figure 1b) were gathered, while in the "Normal" group, the residual time points were included. For each group, the outgoing degrees for each node from "A" to "B" were combined. As shown in Figure 2, (a) represents the results for the "Anomaly" group, and (b) those for the "Normal" group. The darker the color is, the stronger the outgoing degrees will be. By calculating the differences between both groups, two regions with strengthened connections from "A" to "B" are revealed (Figure 2c). The western one (approximately $144^oE \sim 172^oE$, $34^oN \sim 42^oN$) is close to the Kuroshio Extension (KE) and the mixed water region (MWR) between KE and the Oyashio frontal, while the eastern one (approximately $172^oE \sim 156^oW$, $26^oN \sim 38^oN$) is close to the subtropical oceanic frontal (STF). It has been widely suggested that the SSTAs in the KE and Oyashio frontal region are closely connected to variations in the PDO (Frankignoul et al., 2011; Newman et al., 2016), and the STF is also considered as one center of action of the PDO (Nakamura et al., 1997). In particular, it has been found that the vertically averaged ocean temperatures over the upper 300 m in these regions are predictable for several years (Mochizuki et al., 2010). Therefore, the enhanced outgoing degrees in these regions may correspond to a substantial signal in the process of a PDO phase transition. However, the question is, if there is indeed a signal that "propagates" from "A" to "B" a few years before a PDO phase transition, why was this not detected in previous studies? To address this question, for each node in "A", (a) the number of negative outgoing-links and (b) the average link strength are calculated (Equations 4 and 5). Compared to the "Normal" group (Figures 2e and 2h), we found that more negative outgoing-links were built in the "Anomaly" group (Figures 2d and 2f), but the average link strength was not significantly increased (Figures 2g and 2i).

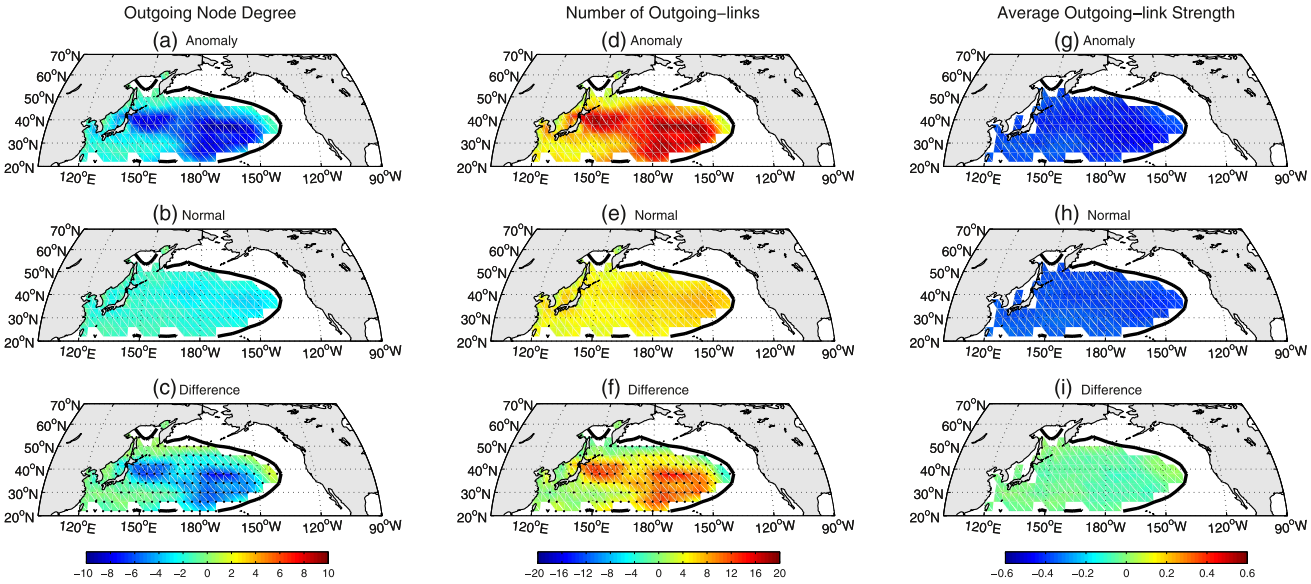

Figure 2. Composite analysis of the outgoing degrees (a–c), the number of outgoing-links (d–f), and the average outgoing-link strength (g–i) for each node in region "A". The first row shows the results for the anomaly group, which gathers the time points with $TD_{A\to B}$ lower than the thresholds (see Figure 1b). The second row represents the results for the normal group, which include all the other time points. The third row shows the differences of the outgoing degrees (c), the number of outgoing-links (f), and the average outgoing-link strength (i) between the anomaly group and the normal group. The black dots mark the nodes with significant differences at the confidence level of 0.01. Obviously, the changes of the outgoing degrees in region "A" are mainly attributed to the changes of the outgoing-link number, not to the changes of each link strength.

This means that the enhanced connections from "*A*" to "*B*" were primarily attributed to an increase in the link number (Figures 2d and 2f), but not to an enhancement of each link strength. As a result, it is difficult to detect this signal using traditional approaches, since the link strength stayed nearly unchanged in the "Anomaly" group. In contrast, due to the advantage of climate network analysis, this signal can be captured due to the enhanced cooperative behavior (i.e., more negative links were built pointing from "*A*" to "*B*"). The same analysis was also performed for the nodes in "*B*", and similar results are found (Figure S9). When studying the incoming degrees, the area along the northwest coast of the Americas was highlighted, indicating the signal propagated from "*A*", would mainly arrive at the northwest coast of the Americas in "*B*".

To further understand the enhanced connections from "*A*" to "*B*" several years before a PDO phase transition, a potential mechanism will be now investigated. Recent studies have reported that a build-up of off-equatorial upper ocean heat content (OEOHC) anomalies in the western tropical Pacific is necessary for a phase transition of the Interdecadal Pacific Oscillation (IPO) (Meehl & Hu, 2006; Farneti et al., 2014). When the vertically integrated heat content to the 20°C isotherm reaches a threshold, an El Niño (La Niña) event could trigger a transition of the IPO toward a positive (negative) phase (Meehl et al., 2016). The associated mechanism has been described in terms of tropical-midlatitude interaction, where the tropical SSTA, westward ocean Rossby waves (near 25°N), and the eastward equatorial ocean Kelvin waves, etc., are key processes to maintain the oscillation. This theory was supported for the IPO phase transition events in late 1970 and late 1990, when the 1976–1977 El Niño event and the 1998–2000 La Niña event triggered the subsequent IPO phase transitions (Meehl et al., 2016). Since the PDO is normally considered as the north Pacific counterpart of the IPO (Henley, 2017; Cassou et al., 2018), although they are not completely identical, it can still be assumed that the same mechanism applies to the phase transition of the PDO, in which case the OEOHC anomalies in the northwestern tropical Pacific (i.e., 5°N–30°N, 125°E–180°E) need to be carefully considered. In this theory, one key point is to monitor whether the OEOHC anomalies in the northwestern tropical Pacific are approaching the threshold. However, this was determined rather subjectively from only one sample (i.e., 2.6×10^{24} J/2.4×10^{24} J for the transition toward the positive/negative phase) in Meehl et al. (2016). Therefore, to improve PDO phase transition forecasts, it is important to determine the threshold more objectively. In this study, a fascinating finding is that the early warning signal detected from climate network analysis (Figure 1b) corresponds very well to the threshold of the OEOHC anomalies, which is

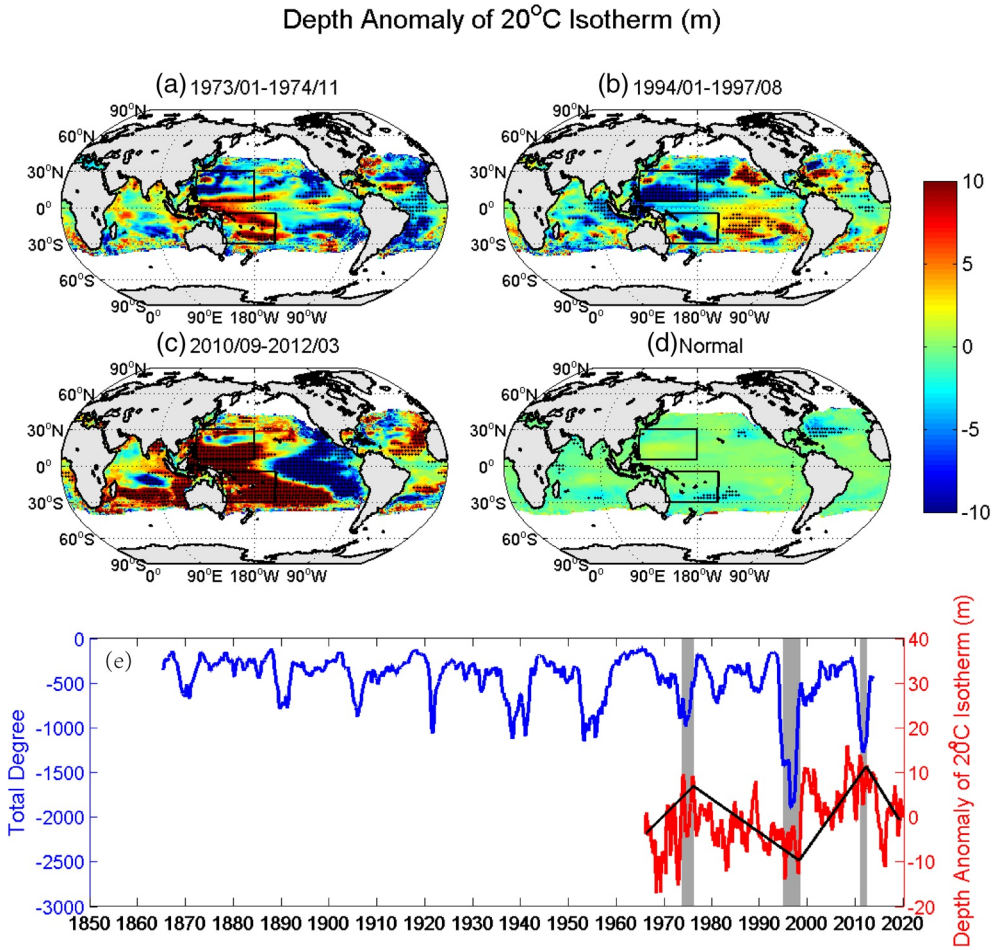

Figure 3. Depth anomalies of the 20°C isotherm compared to 1965–2018 as a reference period (a–c) Show the composite results for the periods 1973/01–1974/11, 1994/01–1997/08, and 2010/09–2012/03, respectively. During these three periods, the $TD_{A\to B}$ was found lower than the thresholds as shown in Figure 1b. In (d), composite results from normal period with $TD_{A\to B}$ above the thresholds are shown. The black dots mark the nodes with significant nonzero depth anomalies at the confidence level of 0.01. The two boxes in (a–d) show the key regions in the northwestern tropical Pacific (5°N–30°N, 125°E–180°E) and the southwestern tropical Pacific (5°S–30°S, 150°E–160°W) as reported in (Meehl et al., 2016). By averaging the depth anomalies in the key region of the northwestern tropical Pacific (the red curve in (e)), close connections between the depth anomalies and the $TD_{A\to B}$ (the blue curve in (e)) are found. The gray bars in (e) represent the periods corresponding to the panels (a)–(c), and divide the red curve into four sections. The black lines indicate the trends from the starting points to the ending points for each section.

represented by the depth of the 20°C isotherm in this work. As reported in Rebert et al. (1985), the ocean heat content vertically integrated to a given isotherm is highly proportional to the depth of the isotherm. In Figure 3, using the latest published sea subsurface temperature data from 1965 to 2018, one can see clearly that the turning points of the depth of the 20° C isotherm in the region 5°N–30°N, 125°E–180° occurred around the time when the early warning signal was detected. This early warning signal was detected from the SSTA, but using sea subsurface temperature data one can obtain similar signals (Figure S10), indicating potential physical linkages between the ocean heat content (OHC) anomalies and the early warning signal. In fact, after the OEOHC in the western tropical Pacific reaches its local maximum/minimum values, even before the next ENSO event there is already an early release of the ocean heat in the following 1–2 years. The accompanying dipole changes in the PDO region (e.g., see Figures S11 and S12) further contribute to the enhancement of the negative connections between "*A*" and "*B*", and induce an enhanced $TD_{A\to B}$. During the time when the OEOHC is not at its local maximum/minimum values, however, the OHC does not show remarkable changes (e.g., see Figures S13 and S14), thus cannot lead to an enhanced $TD_{A\to B}$. Compared to the situations when the phase transition of the PDO has been triggered by the "next" El Niño (La Niña)

event event, here the early warning signals mainly describes the status of the system when the OEOHC anomalies at the western boundary were well built-up, and the associated signals, for example, ocean layer thickness anomalies, start to propagate to the equatorial tropics, produce equatorial ocean Kelvin waves, and connect the two regions "*A*" and "*B*". Accordingly, the signal is weak and hard to detect, which in turn highlights the advantages of the climate network analysis. Since the detection of the early warning signal may serve as an objective judgment on whether the OEOHC anomaly has reached its threshold, we thus propose a new strategy for the prediction of the PDO phase transition. That is, one can first monitor the $TD_{A\to B}$ (as shown in Figure 1b) to see if there is a sudden strengthening of the connections between "*A*" and "*B*". When the early warning signal is detected, a PDO phase transition can then be expected with the arising of the next El Niño (La Niña) event. Based on this strategy, the detected early warning signal in 2010–2012 indicates a potential PDO phase transition after the strong El Niño events in 2015–2016, which is in line with the judgment by (Meehl et al., 2016).

4. Discussion and Conclusions

In this study, we detected an early warning signal for the PDO phase transition using climate network analysis. This signal arises from the cooperative behaviors among a large number of interior grid points in the network, indicating that there is a moment when many grid points in the network behave similarly before the PDO phase transition. Taking this feature, all six PDO phase transitions from 1890 to 2000 were correctly warned, and there is only one false alarm sounded in the middle of the 1950. By calculating the Heidke Skill Score (HSS, Boers et al., 2014) (see Text S1 in the supporting information), we obtain $HSS = 0.92$ for the period from 1889 to 2000 (Table S1), indicating the sudden strengthening of the connections between the two regions ("*A*" and "*B*") can be used as a reliable signal to forewarn the PDO phase transition, and the skill is robust to the selection of different thresholds (see the blue dashed lines in Figures 1b and Figure S15).

In addition to detecting this early warning signal, a more challenging question is how to understand it from a climatic perspective? One may ask whether the early warning signal represents one aspect of the slow phase transition of the PDO as it always appears after the peak of the PDO index (see Figures 1b Figure S16, and Table S2). However, detailed analyses suggest that the signal is more associated with the fast part (e.g., interannual scale) of the PDO. As shown in Figures S17 and S18, a 11-years high-pass filtering of the PDO either use regression-based or EOF-based methods nearly has no impacts on the detection of the early warning signal. In contrast, the removal of the fast part (i.e., 11-years low-pass filtering) makes the early warning signal largely reduced or even vanished. Combining with the fact that the total degrees ($TD_{A\to B}$) are calculated from 5.5 years moving windows, the arising of the pulse-like early warning signal is more likely to be controlled by fast processes on interannual time scale. According to the theories proposed by Meehl et al. (Meehl et al., 2016; Meehl & Hu, 2006), more detailed studies further revealed that the early warning signal arises around the time when the OEOHC anomaly in the western tropical Pacific reaches its threshold. Compared to the triggering effects of ENSO events as suggested by Meehl et al. (Meehl et al., 2016; Meehl & Hu, 2006), this signal is more like an alarm bell that monitors the state when the OEOHC anomalies at the western boundary were well built-up, and the associated signals start to propagate to initiate a PDO phase transition. Accordingly, when this signal is objectively detected, one can expect a PDO phase transition soon with the arising of the next El Niño/La Niña event. This strategy works very well in the hindcast of the PDO phase transition, and underpins the possible PDO phase transition around 2015.

In the end, we would like to note that although the detected early warning signal is physically meaningful, more detailed analyses (including model evaluations) are still needed to fully understand the dynamic mechanisms behind. Recently, it has been reported that the PDO may become less predictable in a warming climate (Li et al., 2020). This calls for more efforts on the PDO prediction research, and more advanced methods are required. Based on the findings of this work, we suggest that the climate network analysis is a powerful approach that deserves more attention in climate studies.

Data Availability Statement

The authors acknowledge the FAIR data policy. The data used here can be downloaded from these links as follows.

ERSST v3b data related to this paper can be accessed at https://www.esrl.noaa.gov/psd/data/gridded/data.noaa.ersst.v3.html

Subsurface temperature data set at different depths can be accessed at http://159.226.119.60/cheng/

Acknowledgments
Many thanks are due to supports from National Key R&D Program of China (2016YFA0600404) and from National Natural Science Foundation of China (No. 41805065 and No. 41675088). N. Yuan thanks also the supports from CAS Pioneer Hundred Talents Program and the Innovation Group Project of Southern Marine Science and Engineering Guangdong Laboratory Zhuhai (No. 311020008). Z. Lu thanks also the supports from CPSF-CAS Joint Foundation for Excellent Postdoctoral Fellows (No. 2017LH012). J. Kurths was supported by the Russian Ministry of Science and Education Agreement No. 075-15-2020-808.

References

Alexander, M. A., Bladé, I., Newman, M., Lanzante, J. R., Lau, N.-C., & Scott, J. D. (2002). The atmospheric bridge: The influence of ENSO teleconnections on air-sea interaction over the global oceans. *Journal of Climate*, *15*(16), 2205–2231. https://doi.org/10.1175/1520-0442(2002)015⟨2205:TABTIO⟩2.0.CO;2

Alexander, M. A., Deser, C., & Timlin, M. S. (1999). The reemergence of SST anomalies in the North Pacific Ocean. *Journal of Climate*, *12*(8), 2419–2431. https://doi.org/10.1175/1520-0442(1999)012⟨2419:TROSAI⟩2.0.CO;2

Boers, N., Bookhagen, B., Barbosa, H. M., Marwan, N., Kurths, J., & Marengo, J. (2014). Prediction of extreme floods in the eastern Central Andes based on a complex networks approach. *Nature Communications*, *5*, 5199. https://doi.org/10.1038/ncomms6199

Boers, N., Goswami, B., Rheinwalt, A., Bookhagen, B., Hoskins, B., & Kurths, J. (2019). Complex networks reveal global pattern of extreme-rainfall teleconnections. *Nature*, *566*(7744), 373–377. https://doi.org/10.1038/s41586-018-0872-x

Boulton, C. A., & Lenton, T. M. (2015). Slowing down of North Pacific climate variability and its implications for abrupt ecosystem change. *Proceedings of the National Academy of Sciences*, *112*(37), 11496–11501. https://doi.org/10.1073/pnas.1501781112

Cai, W., & van Rensch, P. (2012). The 2011 southeast Queensland extreme summer rainfall: A confirmation of a negative Pacific Decadal Oscillation phase? *Geophysical Research Letters*, *39*(8), L08702. https://doi.org/10.1029/2011GL050820

Cassou, C., Kushnir, Y., Hawkins, E., Pirani, A., Kucharski, F., Kang, I.-S., et al. (2018). Decadal climate variability and predictability: Challenges and opportunities. *Bulletin of the American Meteorological Society*, *99*(3), 479–490. https://doi.org/10.1175/BAMS-D-16-0286.1

Cheng, L., Trenberth, K. E., Fasullo, J., Boyer, T., Abraham, J., & Zhu, J. (2017). Improved estimates of ocean heat content from 1960 to 2015. *Science Advances*, *3*(3), e1601545. https://doi.org/10.1126/sciadv.1601545

Chylek, P., Dubey, M. K., Lesins, G., Li, J., & Hengartner, N. (2014). Imprint of the Atlantic multi-decadal oscillation and Pacific decadal oscillation on southwestern US climate: Past, present, and future. *Climate Dynamics*, *43*(1–2), 119–129. https://doi.org/10.1007/s00382-013-1933-3

Dai, A., Fyfe, J. C., Xie, S.-P., & Dai, X. (2015). Decadal modulation of global surface temperature by internal climate variability. *Nature Climate Change*, *5*(6), 555–559. https://doi.org/10.1038/nclimate2605

Deser, C., Phillips, A. S., & Hurrell, J. W. (2004). Pacific interdecadal climate variability: Linkages between the tropics and the North Pacific during boreal winter since 1900. *Journal of Climate*, *17*(16), 3109–3124. https://doi.org/10.1175/1520-0442(2004)017⟨3109:PICVLB⟩2.0.CO;2

Doblas-Reyes, F. J., Andreu-Burillo, I., Chikamoto, Y., Garca-Serrano, J., Guemas, V., Kimoto, M., et al. (2013). Initialized near-term regional climate change prediction. *Nature Communications*, *4*, 1715. https://doi.org/10.1038/ncomms2704

Farneti, R. (2017). Modeling interdecadal climate variability and the role of the ocean. *Wiley Interdisciplinary Reviews: Climate Change*, *8*(1), e441. https://doi.org/10.1002/wcc.441

Farneti, R., Molteni, F., & Kucharski, F. (2014). Pacific interdecadal variability driven by tropical-extratropical interactions. *Climate Dynamics*, *42*(11–12), 3337–3355. https://doi.org/10.1007/s00382-013-1906-6

Feng, Q. Y., Viebahn, J. P., & Dijkstra, H. A. (2014). Deep ocean early warning signals of an Atlantic MOC collapse. *Geophysical Research Letters*, *41*(16), 6009–6015. https://doi.org/10.1002/2014GL061019

Frankignoul, C., Sennéchael, N., Kwon, Y.-O., & Alexander, M. A. (2011). Influence of the meridional shifts of the Kuroshio and the Oyashio Extensions on the atmospheric circulation. *Journal of Climate*, *24*(3), 762–777. https://doi.org/10.1175/2010JCLI3731.1

Henley, B. J. (2017). Pacific decadal climate variability: Indices, patterns and tropical-extratropical interactions. *Global and Planetary Change*, *155*, 42–55. https://doi.org/10.1016/j.gloplacha.2017.06.004

Henley, B. J., Meehl, G., Power, S. B., Folland, C. K., King, A. D., Brown, J. N., et al. (2017). Spatial and temporal agreement in climate model simulations of the Interdecadal Pacific Oscillation. *Environmental Research Letters*, *12*(4), 044011. https://doi.org/10.1088/1748-9326/aa5cc8

Ishii, M., & Kimoto, M. (2009). Reevaluation of historical ocean heat content variations with time-varying XBT and MBT depth bias corrections. *Journal of Oceanography*, *65*(3), 287–299. https://doi.org/10.1007/s10872-009-0027-7

Landscheidt, T. (2001). *Trends in Pacific decadal oscillation subjected to solar forcing*. Schroeter Institute for Research in Cycles of Solar Activity. Retrieved from http://www.john-daly.com/theodor/pdotrend.htm

Li, S., Wu, L., Yang, Y., Geng, T., Cai, W., Gan, B., et al. (2020). The pacific decadal oscillation less predictable under greenhouse warming. *Nature Climate Change*, *10*, 30–34. https://doi.org/10.1038/s41558-019-0663-x

Liu, Z., & Alexander, M. (2007). Atmospheric bridge, oceanic tunnel, and global climatic teleconnections. *Reviews of Geophysics*, *45*(2), RG2005. https://doi.org/10.1029/2005RG000172

Ludescher, J., Gozolchiani, A., Bogachev, M. I., Bunde, A., Havlin, S., & Schellnhuber, H. J. (2013). Improved El Niño forecasting by cooperativity detection. *Proceedings of the National Academy of Sciences*, *110*(29), 11742–11745. https://doi.org/10.1073/pnas.1309353110

Mantua, N. J., & Hare, S. R. (2002). The pacific decadal oscillation. *Journal of Oceanography*, *58*(1), 35–44. https://doi.org/10.1023/A:1015820616384

Mantua, N. J., Hare, S. R., Zhang, Y., Wallace, J. M., & Francis, R. C. (1997). A Pacific interdecadal climate oscillation with impacts on salmon production. *Bulletin of the American Meteorological Society*, *78*(6), 1069–1079. https://doi.org/10.1175/1520-0477(1997)078⟨1069:APICOW⟩2.0.CO;2

Medhaug, I., Stolpe, M. B., Fischer, E. M., & Knutti, R. (2017). Reconciling controversies about the global warming hiatus. *Nature*, *545*(7652), 41–47. https://doi.org/10.1038/nature22315

Meehl, G. A., & Hu, A. (2006). Megadroughts in the Indian monsoon region and southwest north America and a mechanism for associated multi-decadal Pacific sea surface temperature anomalies. *Journal of Climate*, *19*(9), 1605–1623. https://doi.org/10.1175/JCLI3675.1

Meehl, G. A., Hu, A., & Teng, H. (2016). Initialized decadal prediction for transition to positive phase of the Interdecadal Pacific Oscillation. *Nature Communications*, *7*(1), 11718. https://doi.org/10.1038/ncomms11718

Meehl, G. A., Teng, H., & Arblaster, J. M. (2014). Climate model simulations of the observed early-2000 hiatus of global warming. *Nature Climate Change*, *4*(10), 898–902. https://doi.org/10.1038/nclimate2357

Meng, J., Fan, J., Ludescher, J., Agarwal, A., Chen, X., Bunde, A., et al. (2020). Complexity-based approach for El Niño magnitude forecasting before the spring predictability barrier. *Proceedings of the National Academy of Sciences*, *117*(1), 177–183. https://doi.org/10.1073/pnas.1917007117

Mochizuki, T., Ishii, M., Kimoto, M., Chikamoto, Y., Watanabe, M., Nozawa, T., et al. (2010). Pacific decadal oscillation hindcasts relevant to near-term climate prediction. *Proceedings of the National Academy of Sciences*, *107*(5), 1833–1837. https://doi.org/10.1073/pnas.0906531107

Nakamura, H., Lin, G., & Yamagata, T. (1997). Decadal climate variability in the North Pacific during the recent decades. *Bulletin of the American Meteorological Society*, *78*(10), 2215–2225. https://doi.org/10.1175/1520-0477(1997)078⟨2215:DCVITN⟩2.0.CO;2

Newman, M., Alexander, M. A., Ault, T. R., Cobb, K. M., Deser, C., Di Lorenzo, E., et al. (2016). The pacific decadal oscillation, revisited. *Journal of Climate*, *29*(12), 4399–4427. https://doi.org/10.1175/JCLI-D-15-0508.1

Newman, M., Compo, G. P., & Alexander, M. A. (2003). ENSO-forced variability of the Pacific Decadal Oscillation. *Journal of Climate*, *16*(23), 3853–3857. https://doi.org/10.1175/1520-0442(2003)016%3c3853:EVOTPD%3d2.0.CO;2

Pierce, D. W. (2001). Distinguishing coupled ocean-atmosphere interactions from background noise in the North Pacific. *Progress in Oceanography*, *49*(1–4), 331–352. https://doi.org/10.1016/S0079-6611(01)00029-5

Qian, C., & Zhou, T. (2013). Multidecadal variability of north china aridity and its relationship to PDO during 1900-2010. *Journal of Climate*, *27*(3), 1210–1222. https://doi.org/10.1175/JCLI-D-13-00235.1

Radebach, A., Donner, R. V., Runge, J., Donges, J. F., & Kurths, J. (2013). Disentangling different types of El Niño episodes by evolving climate network analysis. *Physical Review E*, *88*(5), 052807. https://doi.org/10.1103/PhysRevE.88.052807

Rebert, J. P., Donguy, J. R., Eldin, G., & Wyrtki, K. (1985). Relations between sea level, thermocline depth, heat content, and dynamic height in the tropical Pacific Ocean. *Journal of Geophysical Research Oceans*, *90*(C6), 11719. https://doi.org/10.1029/jc090ic06p11719

Schneider, N., & Cornuelle, B. D. (2005). The forcing of the Pacific decadal oscillation. *Journal of Climate*, *18*(21), 4355–4373. https://doi.org/10.1175/JCLI3527.1

Sheffield, J., Camargo, S. J., Fu, R., Hu, Q., Jiang, X., Johnson, N., et al. (2013). North American climate in CMIP5 experiments. Part II: Evaluation of historical simulations of intraseasonal to decadal variability. *Journal of Climate*, *26*(23), 9247–9290. https://doi.org/10.1175/JCLI-D-12-00593.1

Smith, T. M., Reynolds, R. W., Peterson, T. C., & Lawrimore, J. (2008). Improvements NOAAs Historical Merged Land-Ocean Temp Analysis (1880-2006). *Journal of Climate*, *21*(10), 2283–2296. https://doi.org/10.1175/2007JCLI2100.1

Tsonis, A. A., Swanson, K. L., & Roebber, P. J. (2006). What do networks have to do with climate? *Bulletin of the American Meteorological Society*, *87*(5), 585–595. https://doi.org/10.1175/BAMS-87-5-585

van der Mheen, M., Dijkstra, H. A., Gozolchiani, A., Den Toom, M., Feng, Q., Kurths, J., et al. (2013). Interaction network based early warning indicators for the Atlantic MOC collapse. *Geophysical Research Letters*, *40*(11), 2714–2719. https://doi.org/10.1002/grl.50515

Yang, Q., Ma, Z., & Xu, B. (2017). Modulation of monthly precipitation patterns over East China by the Pacific Decadal Oscillation. *Climatic Change*, *144*(3), 405–417. https://doi.org/10.1007/s10584-016-1662-9